

PAPER

View Article Online
View Journal | View Issue



CrossMark
click for updates

Cite this: *Environ. Sci.: Processes
Impacts*, 2014, **16**, 2137

Uranium incorporation into aluminum-substituted ferrihydrite during iron(II)-induced transformation†

Michael S. Massey,^{‡*a} Juan S. Lezama-Pacheco,^{ac} F. Marc Michel^b
and Scott Fendorf^{*a}

Uranium retention processes (adsorption, precipitation, and incorporation into host minerals) exert strong controls on U mobility in the environment, and understanding U retention is therefore crucial for predicting the migration of U within surface and groundwater. Uranium can be incorporated into Fe (hydr)oxides during Fe(II)-induced transformation of ferrihydrite to goethite. However, ferrihydrite seldom exists as a pure phase within soils or sediments, and structural impurities such as Al alter its reactivity. The presence of Al in ferrihydrite, for example, decreases the rate of transformation to goethite, and thus may impact the retention pathway, or extent of retention, of U. Here, we investigate the extent and pathways of U(VI) retention on Al-ferrihydrite during Fe(II)-induced transformation. Ferrihydrite containing 0%, 1%, 5%, 10%, and 20% Al was reacted with 10 μ M U and 300 μ M Fe(II) in the presence of 0 mM and 4 mM Ca^{2+} and 3.8 mM carbonate at pH 7.0. Solid reaction products were characterized using U $L_{3\text{-edge}}$ EXAFS spectroscopy to differentiate between adsorbed U and U incorporated into the goethite lattice. Uranium incorporation into Al-ferrihydrite declined from $\sim 70\%$ of solid-phase U at 0% and 1% Al to $\sim 30\%$ of solid phase U at 20% Al content. The decrease in U incorporation with increasing Al concentration was due to two main factors: (1) decreased transformation of ferrihydrite to goethite; and, (2) a decrease of the goethite lattice with increasing Al, making the lattice less compatible with large U atoms. However, uranium incorporation can occur even with an Al-substituted ferrihydrite precursor in the presence or absence of Ca^{2+} . The process of U incorporation into Al-goethite may therefore be a potential long-term sink of U in subsurface environments where Al-substituted iron oxides are common, albeit at lower levels of incorporation with increasing Al content.

Received 10th March 2014

Accepted 7th August 2014

DOI: 10.1039/c4em00148f

rsc.li/process-impacts

Environmental impact

Uranium exerts a threat to surface and groundwater across the globe owing to both anthropogenic activities, such as mining and nuclear fuel production, as well as natural sources. Iron oxides serve as principal hosts of uranium through adsorption and co-precipitation pathways, with the ubiquitous iron phase ferrihydrite serving a particularly prominent, and unique, role in uranium retention. Here we examine the unresolved influence of chemical heterogeneities in ferrihydrite composition on uranium retention upon reaction with Fe(II) (common under anaerobic conditions). We observed that uranium incorporation into the Al-ferrihydrite transformation product, goethite, declined from $\sim 70\%$ of solid-phase U without Al to $\sim 30\%$ with 20% Al content. Thus, Al within ferrihydrite diminishes a reaction pathway serving as a long-term host of uranium.

1. Introduction

Uranium mining, milling, and refining, as well as nuclear weapon and fuel production, have left a substantial legacy of

soil and groundwater contamination. Uranium contamination from legacy U production exists on every continent except Antarctica, with an estimated global volume of over 900 million m^3 of U mine/mill tailings. These occupy a land area of nearly 6000 ha, and occur with associated contamination of soils, sediments, and groundwater.¹ As one example, the United States Department of Energy manages an inventory of 1.5 billion m^3 of contaminated groundwater, and 75 million m^3 of contaminated soil/sediment,² and U is among the most common radionuclide contaminants at United States DOE sites.³ Managing U contamination requires an accurate understanding of U biogeochemical processes and retention mechanisms. Thus, establishing a clearer understanding of U biogeochemistry is crucial for mitigating the impact of legacy contamination, as

^aDepartment of Environmental & Earth System Science, Stanford University, Stanford, California 94305, USA

^bVirginia Polytechnic Institute and State University, Blacksburg, Virginia 24061, USA

^cSLAC National Accelerator Laboratory, Menlo Park, California 94025, USA

† Electronic supplementary information (ESI) available. See DOI: 10.1039/c4em00148f

‡ Present address: Department of Earth and Environmental Sciences, California State University East Bay, 25800 Carlos Bee Boulevard, Hayward, California 94542, USA. E-mail: mike.massey@csueastbay.edu; Tel: +1-510-885-3486.

well as understanding current and future environmental impacts of U.

Three U retention processes have been the subject of intensive study over the past several decades: (1) U(vi) adsorption to soil and sediment solids, (2) reduction of U(vi) in groundwater to sparingly-soluble U(iv) solids, and, most recently, (3) incorporation of U(vi/v) into iron oxides such as hematite,^{4,5} goethite,^{6–8} and possibly magnetite.⁶ The uranyl cation (UO_2^{2+}) can adsorb on iron oxide, hydroxide, and oxyhydroxide minerals, hereafter referred to collectively as “iron oxides”.^{9–12} Uranyl also adsorbs on clay minerals¹³ and quartz.¹⁴ As a long-term retention mechanism, however, adsorption may be limited due to the reversible nature of adsorption reactions with shifts in aqueous chemistry. An increase in Ca^{2+} and carbonate concentrations, for example, can lead to the formation of uranyl–calcium–carbonate ternary complexes which decrease the extent of adsorption and promote desorption.^{15,16}

Uranium(vi) reduction to sparingly-soluble U(iv) solids such as uraninite (UO_2) and “monomeric” U(iv) species is another potential U retention pathway. There are a variety of abiotic and biotic pathways of U(vi) reduction, including reaction with Fe(II), hydrogen sulfide, or Fe(II)-bearing solids such as magnetite.^{17–20} Ferrous iron has been shown to reduce U(vi) either through a heterogeneous reaction mediated by, for example, iron oxide surfaces¹⁷ or homogeneously in aqueous solution.²¹ In addition to abiotic reductants of aqueous U(vi), biotic pathways have been examined extensively. They have been used in U contamination remediation *via in situ* biostimulation of metal reducing microorganisms.^{22–27} Independent of its formation pathway, U(iv) can persist for long periods of time, such as in U-bearing roll-front deposits. However, re-oxidation and subsequent re-mobilization of U by dissolved oxygen,²⁸ dissolved nitrate,^{29–31} or Fe(III) and Mn(IV/III) minerals^{32,33} is a concern. The dependence of U reduction on aqueous U speciation, and the potential for re-oxidation/remobilization, make the effectiveness of reductive retention dependent on stable long-term geochemical conditions.

Uranium(vi/v) incorporated into iron oxides, on the other hand, is resistant to release upon pH change,⁷ oxidizing conditions, and short-period redox cycling.³⁴ Uranium(vi) incorporated in hematite^{4,5} and U(v) in goethite^{6–8,35} is present in uranate (octahedral) coordination, rather than uranyl coordination (UO_2^{2+}) of the dominant aqueous and adsorbed U species. Gómez *et al.*³⁶ found that U incorporation or co-precipitation in iron minerals can exert a substantial control over aqueous U concentrations near mine tailings. Additionally, uranium associated with iron oxides may be stable over geologic timescales,³⁷ so U incorporation into iron oxide minerals could serve as a stable, long-term sink for contaminant U.

Uranium retention processes occur concurrently with iron biogeochemical transformations in subsurface environments. For example, the iron hydroxide ferrihydrite can be transformed into the more thermodynamically-favorable products lepidocrocite, goethite, or magnetite by reaction with aqueous Fe(II).^{38–40} Many different parameters affect ferrihydrite transformation, however. For example, Fe(II) concentration, pH changes, and the presence of chloride, sulfate, or carbonate in solution can alter the transformation products,³⁹ while

adsorbates such as phosphate and silicate can inhibit transformation.^{41,42}

Structural impurities in ferrihydrite, such as Al or Si, can also dramatically alter the reactivity of ferrihydrite and its transformation products. Structural Al can be found at concentrations as high as 30% in synthetic or natural samples of iron oxides.^{43–45} Aluminum inhibits ferrihydrite transformation to more-crystalline iron oxides at high Al concentrations.^{46,47} Hansel *et al.*⁴⁷ also found that structural Al influences the reaction products (*e.g.*, lepidocrocite *vs.* goethite), though the specific mechanisms behind the influence of structural Al on reaction products remain unclear. Although structural Si in ferrihydrite was noted to preserve reactivity upon desiccation,⁴² it also inhibited U incorporation during Fe(II)-induced transformation,⁷ highlighting the potential importance of co-precipitated ions such as Si and Al in coupled U and Fe biogeochemical processes. The impact of structural Al on U incorporation has not yet been examined, despite the ubiquitous nature of Al-substituted iron oxide minerals in the environment. The relevance of the U incorporation pathway in natural systems is predicated upon U incorporation into iron oxides that only rarely exist in a pure state. Accordingly, the objective of this study was to elucidate the impact of Al-ferrihydrite on U incorporation during Fe(II)-induced ferrihydrite transformation.

2. Methods

In order to test the influence of Al on U incorporation into Al-containing ferrihydrite, ferrihydrite slurries with 0%, 1%, 5%, 10%, and 20% (hereafter, “Al-ferrihydrite”) were synthesized. The Al-ferrihydrite slurry was then reacted with U and Fe(II) at pH 7.0 to induce Al-ferrihydrite transformation and U incorporation.

2.1. Synthesis of Al-ferrihydrite slurry

Stock solutions of 150 μM FeCl_3 and AlCl_3 were combined proportionally for Al mole percentages of 0%, 1%, 5%, 10%, and 20%. The combined solutions were stirred continuously and vigorously while undergoing rapid (<10 minutes) hydrolysis using 1 M NaOH to bring the final pH to 7.2–7.3. The supernatant was decanted and the slurry was centrifuged at 6000 RPM and washed with de-ionized water (18 M Ω) five times to remove excess salt. The method was similar to that in Masue *et al.*⁴⁸ The final slurries were sampled under vigorous stirring, dissolved with 6 M trace metal grade HCl, and analyzed with inductively-coupled plasma optical emission spectrometry (ICP-OES) to obtain Fe and Al concentrations. X-ray powder diffraction illustrated an Al-ferrihydrite diffraction pattern consistent with 2-line ferrihydrite.

2.2. Batch incubation experiments

Batch incubations were performed in 125 mL glass serum bottles with thick rubber stoppers (Bellco Glass, Inc., New Jersey, USA). A total of 100 mL of solution and slurry was added to serum bottles in a 95% N_2 /5% H_2 atmosphere (Coy Laboratory

Products, Michigan, USA). The solution consisted of 10 mM PIPES buffer and 3.8 mM KHCO_3 , adjusted to pH 7.0 with trace metal grade HCl. Either 0 mM or 4 mM Ca^{2+} (added as $\text{CaCl}_2 \cdot 2\text{H}_2\text{O}$) was used to examine the effect of uranyl–calcium–carbonato complexation, and 0 or 10 μM U (as uranyl acetate) provided both U-containing samples and no-U controls. The 10 μM U concentration was chosen as a reasonable model for U contamination in groundwater, which often ranges from 10^{-7} M to 10^{-4} M. Solutions were made using de-ionized water (18 M Ω) that had been de-oxygenated by boiling and bubbling with a stream of N_2 gas for several hours.

(Al-)ferrihydrite was added to each bottle in an amount based on the ferrihydrite slurry density, in order to achieve a final Fe + Al concentration of ~ 1.7 mM (equivalent to 15–20 mg of Al-ferrihydrite per bottle, or a solid concentration of ~ 150 –200 mg L^{-1}). Then, uranyl acetate was added for a concentration of either 0 μM or 10 μM . This mixture was capped and sealed using thick rubber stoppers, and allowed to equilibrate for ~ 1 h. Finally, 0.3 mL of 100 mM FeSO_4 was added using a needle and syringe for an initial Fe(II) concentration of 300 μM . The addition of Fe(II) initiated ferrihydrite and U transformation. Uranium-containing incubations were performed in triplicate.

Capped, anoxic samples were incubated at 25 °C for 7–8 days on a rotary shaker at 120 RPM. After incubation, duplicate 10 mL aliquots of solution were withdrawn using a needle and syringe, and filtered through 0.22 μm nitrocellulose membranes into 15 mL serum vials. These vials were capped for storage and chemical analysis. The remainder of each sample (~ 80 mL) was vacuum-filtered through a 0.22 μm nitrocellulose membrane, scraped from the filter while wet, washed 3–5 times with de-ionized water, air-dried, and ground for analysis. Solution and solid sampling were performed under a 95% N_2 /5% H_2 atmosphere.

2.3. Solution analysis

Aliquots of solutions were diluted using 3% trace metal grade HNO_3 for chemical analysis. Uranium was measured using inductively-coupled plasma mass spectrometry (ICP-MS, Thermo Scientific XSERIES 2, Thermo Fisher Scientific, Waltham, MA), and Fe, Ca, K, Na, and Al were measured using inductively-coupled plasma optical emission spectrometry (ICP-OES, Thermo Scientific ICAP 6300 Dual View, Thermo Fisher Scientific, Waltham, MA).

2.4. Solid analysis

2.4.1. X-ray absorption spectroscopy. Uranium $\text{L}_{3\text{-edge}}$ and Fe K-edge X-ray absorption spectra were collected at beamlines 11-2 and 4-1 at the Stanford Synchrotron Radiation Lightsource (SSRL). Dried solid powder (~ 15 mg) was diluted with deoxygenated BN powder (~ 70 mg) and homogenized by grinding with an agate mortar and pestle. Samples were sealed with three layers of Kapton film, and placed under vacuum to isolate the samples from oxygen during analysis at room-temperature. The X-ray beam incident energy was controlled using a Si(220) double crystal monochromator in the $\Phi = 0^\circ$ orientation (for U) and $\Phi = 90^\circ$ orientation (for Fe). An in-line Y or Fe foil was used

for energy calibration; the Y K-edge was calibrated to 17038.4 eV, and the Fe K-edge was calibrated to 7111.0 eV. Transmission spectra were collected using an in-line ion chamber, and fluorescence spectra were collected simultaneously with either a 13- or 30-element Ge solid-state detector (Canberra, Connecticut, USA) for U, or a Lytle detector for Fe.

Data calibration and averaging were performed using Six-Pack.⁴⁹ Background subtraction, normalization, and linear combination fitting analyses were performed with Athena.⁵⁰ Standard spectra for linear combination fits were collected and processed under identical conditions and fit using Artemis and FEFF 6.0 or FEFF 8.4.^{51,52} Detailed normalization and fitting parameters, as well as EXAFS spectra, are given in the ESI.[†] The uncertainty associated with EXAFS linear combination fitting was approximately 5–15%, as detailed in the ESI.[†]

2.4.2. High-resolution synchrotron X-ray powder diffraction. Ground Al/Fe oxide/U powder was placed in 0.3 mm diameter borosilicate glass capillaries (Hampton Research, Aliso Viejo, CA). Capillaries were sealed using five-minute epoxy (ITW Devcon, Danvers, MA, USA) in a 95% N_2 /5% H_2 atmosphere and analyzed at beamline 7-2 at SSRL. Capillaries were contained in sealed plastic containers with Kapton windows for radionuclide containment; the containers were purged with He gas during analysis to minimize oxygen exposure and decrease scattering background. The incident beam energy was maintained at 16.5 keV, and precise calibration was achieved using a powdered LaB_6 calibration standard in a borosilicate glass capillary. High-resolution synchrotron X-ray powder diffraction data were collected over a Q-space range of ~ 0.8 –12 by scanning a Vortex Si solid state detector (SII Nanotechnology USA Inc., Northridge, CA, USA) in steps of $Q = 0.05$.

Diffraction patterns were analyzed using the General Structure Analysis System (GSAS) software package⁵³ with the EXPGUI interface.⁵⁴ Lattice parameters and coherent scattering domain size (nominal crystallite size) were determined using Rietveld refinement. Capillary background and a residual ferrihydrite phase were fit separately and included in the goethite Rietveld refinement in order to accurately refine peak shapes and peak intensities of the goethite diffraction pattern. Instrument-specific and experiment-specific parameters were determined using the LaB_6 diffraction pattern, as in Campbell *et al.*⁵⁵ Lattice parameters and Lorentzian broadening parameters (related to coherent scattering domain size) were then refined. Full details of the refinement are given in ESI.[†]

3. Results

3.1. Uranium solid/solution partitioning

Using batch reactors, we investigated the retention of U(VI) upon Fe(II) reaction with ferrihydrite having varying amounts of structural Al. Increasing levels of Al within ferrihydrite, from 0 to 20 mol%, decreased the extent of U retention (Fig. 1). Uranium retention was further diminished by the presence of Ca^{2+} . With Ca^{2+} in solution, U retention decreased by an order of magnitude compared to the no-Ca system. More specifically, in the system with Ca, U in solution increased from 4% (0% Al-ferrihydrite) to 16% (1% Al-ferrihydrite) and up to >30% (20%

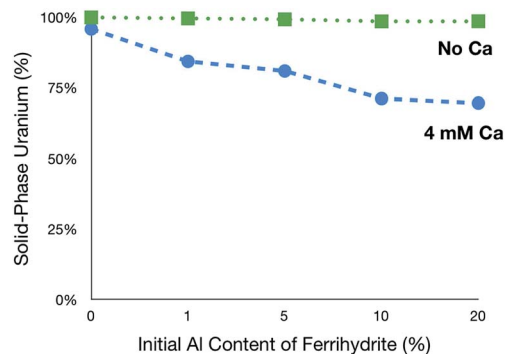


Fig. 1 Uranium partitioned into the solid phase as a function of Al content of initial ferrihydrite slurry (0–20 mol% Al substitution for Fe). Incubations were performed with an initial $U(vi)_{(aq)}$ concentration of 10 μM , in the presence or absence of $Ca^{2+}_{(aq)}$ (0 mM or 4 mM Ca), upon reaction with (Al-)ferrihydrite slurry, 0.3 mM Fe(II), and 3.8 mM carbonate at a pH of 7.0. Error bars are smaller than the data symbols.

Al-ferrihydrite). In the absence of Ca, the trend of increasing solution-phase U with increasing Al in the solid generally held, but the impact was small and in all cases greater than 98% of U was associated with the solid phase (Fig. 1).

3.2. Uranium solid phase speciation

Uranium L_{3-} edge EXAFS linear combination fitting was performed to determine the proportions of U incorporated in *versus* adsorbed on the Al-ferrihydrite transformation products (Fig. 2). Greater amounts of Al in ferrihydrite decreased U incorporation into transformation products (Fig. 3). With 4 mM Ca^{2+} , the 0% and 1% Al-ferrihydrite transformation products were very similar, with 72% and 63% incorporated U, respectively. The 5% and 10% Al-ferrihydrite transformation products

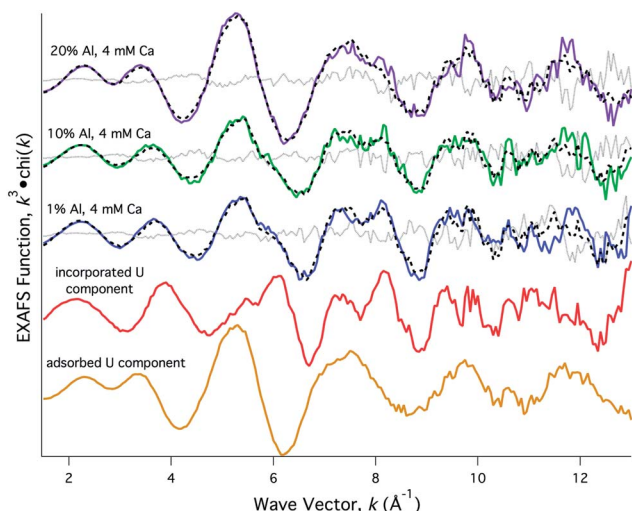


Fig. 2 EXAFS linear combination fitting results for k^3 -weighted U L_{3-} edge EXAFS spectra for Al-ferrihydrite (0–20 mol% Al substituted for Fe) reacted with 10 μM U(VI), 0.3 mM Fe(II), 3.8 mM carbonate, and 0 mM Ca, at pH 7.0. Data (colored lines), fitting components (incorporated U, adsorbed U), linear combination fits (black dotted lines), and residuals (light grey dotted lines) are shown.

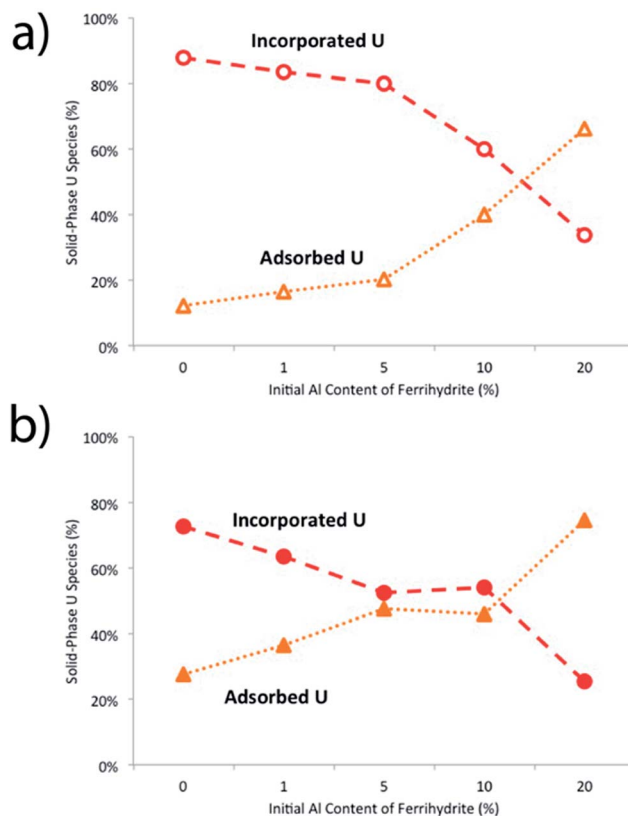


Fig. 3 Solid phase U speciation as a function of initial Al content of ferrihydrite slurry (0–20 mol% Al substitution for Fe) after reaction with 10 μM initial $U(vi)_{(aq)}$, 0.3 mM Fe(II), 3.8 mM carbonate at pH 7.0 and (a) 0 mM Ca, or (b) 4 mM Ca. Linear combination fitting EXAFS percent-ages are shown for incorporated U(VI) (red circles) and adsorbed U(VI) (yellow triangles).

contained 52% and 54% incorporated U, respectively, while the 20% Al-ferrihydrite transformation product contained 25% incorporated U and 75% adsorbed U (Fig. 3a). Calcium decreased the proportion of incorporated U and decreased the proportion of adsorbed U at all Al loadings. No U(IV) solids, such as UO_2 , were observed *via* EXAFS spectroscopy.

Taken together, the U retention (Fig. 1) and EXAFS linear combination fitting results (Fig. 2 and 3) indicate that most of the U in the system was incorporated into the goethite solid (see below for iron oxide transformation products) at 0% and 1% Al contents, regardless of Ca^{2+} presence or absence. However, with increasing Al content, adsorbed and aqueous U(VI) became more prevalent. This trend was particularly evident in the presence of 4 mM Ca^{2+} , with less than 20% of the U in the system incorporated into the goethite solid at 20% Al content within ferrihydrite. Even with increased U retention in the absence of Ca^{2+} , only about 32% of the initial U was incorporated into the 20% Al-goethite.

3.3. Initial Al-ferrihydrite and coherent scattering domain size

The initial Al-ferrihydrite solids were examined using X-ray diffraction and high-energy total scattering and pair

distribution function (PDF) analysis. Initial materials were all two-line ferrihydrite (Fig. S1†). The PDF of the initial 1–20% Al-ferrihydrite solids were very similar (Fig. S2†), with a coherent scattering domain (CSD) size of ~ 2 nm. There was a slight decrease in CSD with increasing Al content; a similar decrease in CSD (a proxy for particle size) was also observed by Cismasu *et al.*⁴⁵ No separate Al oxide domains or phases were detected using X-ray scattering, but they may have been present in the 20% Al-ferrihydrite.^{45,56}

3.4. Iron oxide transformation products

Crystalline solid phases were identified using high-resolution synchrotron X-ray powder diffraction, and Fe oxides were

further examined using Fe K-edge EXAFS spectroscopy. Goethite was the only crystalline Fe oxide transformation product observed in either the 4 mM Ca or 0 mM Ca systems (Fig. S3†). Rietveld refinement of fits of goethite diffraction patterns indicated that the lattice parameters changed with increasing Al loading (Fig. 4). Typical crystallographic values for pure goethite are $a = 4.61$ Å, $b = 9.96$ Å, and $c = 3.02$ Å.⁴³ However, the a lattice parameter decreased from ~ 4.625 Å to ~ 4.615 Å as Al substitution increased from 1% Al to 20% Al (Fig. 4). Similarly, the b lattice parameter decreased from ~ 9.98 Å to ~ 9.92 Å, and the c lattice parameter decreased from ~ 3.035 Å to ~ 3.010 Å as Al content increased from 1% to 20% (Fig. 4). Iron K-edge EXAFS linear combination fitting indicated that unreacted ferrihydrite accounted for 28% to 48% of the Fe oxide in the Al-ferrihydrite transformation products of the 4 mM Ca^{2+} system; 23–41% remained as ferrihydrite in the no-Ca system (Fig. S4 and S5†).

4. Discussion

Across all Al loadings, with either 4 mM or 0 mM Ca^{2+} , ~ 70 –99% of the U in the system was retained on the solid phase (Fig. 1), consistent with previous findings.^{15,16} The dominance of the uranyl–calcium–carbonato ternary complex in solution decreased U retention at 5–20% Al content. The presence of 4 mM Ca^{2+} , and the corresponding shift of U aqueous speciation to a regime dominated by the uranyl–calcium–carbonato complex, resulted in an order of magnitude more U in the aqueous phase in comparison to the 0 mM Ca^{2+} system (Fig. 1). The decrease of U retention was accompanied by a shift in the dominant solid-phase U retention pathway from U incorporation into goethite to U adsorption on the Al-containing oxides (Fig. 2 and 3). However, an increase in both structural Al in ferrihydrite (and Al in the subsequent goethite transformation product), coupled with a shift in uranyl speciation to the ternary uranyl–calcium–carbonato complex, diminishes U incorporation; with 20% Al content and 4 mM Ca^{2+} , only $\sim 17\%$ of total U is incorporated into goethite.

The dominant effect on the U retention mechanisms under the conditions of this study resulted from the structural Al content of the ferrihydrite precursors and goethite transformation products. An increase in Al content had the overriding effect of decreasing U incorporation and shifting the retention mechanism toward uranyl adsorption. Uranium incorporation into Al-ferrihydrite transformation products decreased from 63–88% in 0% and 1% Al-ferrihydrite to 25–34% with 20% Al-ferrihydrite (Fig. 3). Uranium incorporation into goethite during Fe(II)-induced ferrihydrite transformation proceeds by the reduction of adsorbed U(VI) to U(V) by Fe(II).⁸ There are two possible reasons for the non-linear decrease of U incorporation into goethite and increased dominance of U adsorption in systems with increasing Al content: (1) inhibition of ferrihydrite transformation to goethite (which may be coupled to a limitation in reduction of adsorbed U(VI)); or, (2) structural incompatibility with incorporated U(V) resulting from a smaller crystal lattice in Al-bearing ferrihydrite and goethite. It is also possible that Al creates a greater availability of adsorption sites by limiting ferrihydrite transformation to goethite but

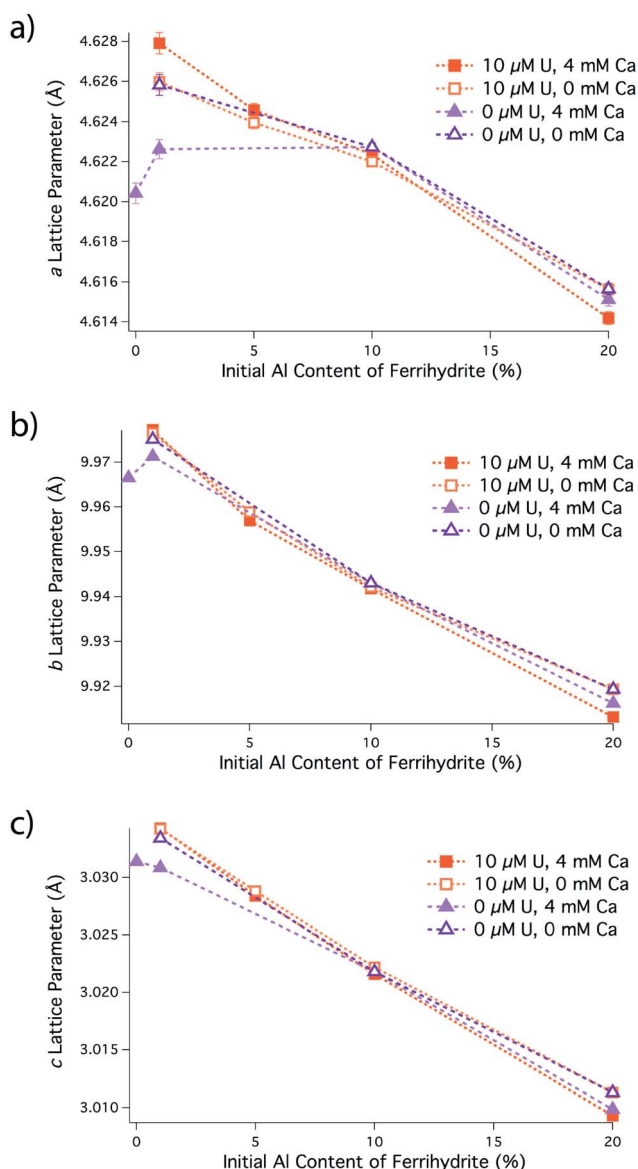


Fig. 4 Lattice parameters of goethite as a function of Al content in ferrihydrite slurry (0–20 mol% Al substituted for Fe). Goethite was the result of the reaction of Al-ferrihydrite slurry with $10 \mu\text{M}$ initial $\text{U(VI)}_{(\text{aq})}$, 0.3 mM Fe(II), 3.8 mM carbonate, and 0 mM Ca or 4 mM Ca, at pH 7.0. Panels a, b, and c correspond to a , b , and c lattice parameters of goethite, respectively.

we do not believe this would limit Fe(II)-induced reductive incorporation of U into goethite.

The first explanation for the decrease in U incorporation is the decreased transformation of ferrihydrite to goethite (Fig. S4†). Formation of goethite *via* Fe(II)-induced transformation of ferrihydrite is necessary for U(V) incorporation.⁸ Masue-Slowey *et al.*⁴⁶ and Hansel *et al.*⁴⁷ both demonstrated that structural Al decreases the extent of Al-ferrihydrite transformation; Masue-Slowey *et al.*⁴⁶ attributed this to inhibition by Al of electron hopping and bulk conduction^{57–60} in the iron oxide structure. Bazilevskaya *et al.*⁵⁶ noted that at Al content greater than 8%, structural Al³⁺ is clustered rather than independently distributed throughout the Fe/Al oxide structure, which further suggests inhibition of electron hopping in the bulk solid, and partially explains the decreased ferrihydrite transformation and U incorporation observed at Al loadings of 10% and 20%. Cismasu *et al.*⁴⁵ also observed Al-rich clusters at Al contents as low as 15%. Masue-Slowey *et al.*⁴⁶ reported only goethite and ferrihydrite products from an Al-ferrihydrite slurry precursor, a finding consistent with the results of the present study.

A second possibility to explain the observed decrease in U incorporation is that of structural limitations caused by Al (and U) in goethite, the dominant transformation product (Fig. S3†). Several investigators have found that U incorporates into octahedral Fe³⁺ sites in goethite.^{6–8} Atomistic modeling supports the possibility of U(V) incorporation in these cation sites, with local charge balance achieved through protonation/de-protonation of nearby hydroxyls, or the introduction of structural vacancies at cation sites.³⁵ However, in addition to local charge balance, lattice parameters and relief of lattice strain are also of concern. Rietveld refinement of high-resolution synchrotron X-ray powder diffraction patterns indicated a decrease in lattice parameters with increasing Al content in goethite (Fig. 4). The presence of Al results in decreased unit cell size in the goethite, due to the smaller size of the Al³⁺ cation with respect to Fe³⁺. ^{VI}U⁵⁺ is a large cation (~0.75–0.80 Å when incorporated in goethite as U⁵⁺) compared to ^{VI}Fe³⁺ (0.65 Å), and certainly compared to ^{VI}Al³⁺ (0.54 Å). Uranium substitution for Fe³⁺/Al³⁺ is likely increasingly less favorable with greater Al in the goethite lattice.

A further contribution to the shift from incorporation to adsorption at higher Al content is the availability of surface sites for uranyl adsorption. At 10–20% Al content, decreased U incorporation into goethite and increased residual ferrihydrite resulted in U retention primarily as an adsorbed species. This may be partly attributed to differences in residual ferrihydrite, in concert with decreased removal of U from solid-solution exchange by U incorporation. Typical N₂-BET surface area of ferrihydrite slurry ranges from 159–234 m² g^{−1},^{61,62} the available surface area of undried slurry is likely even higher due to particle aggregation from drying prior to measurement. Roden and Zachara⁶³ reported goethite surface area ranging from 31 to 153 m² g^{−1}, depending on goethite particle size (100–200 nm to 15–30 nm, respectively). Higher surface area, especially from residual Al-ferrihydrite, will favor U adsorption over U incorporation due to greater availability of adsorption sites. Potentially more important, however, is that U retained on ferrihydrite is not available for reduction to U(V) and

incorporation into the goethite transformation product, since incorporation of U(V) relies on the mineral transformation.

Factors such as aggregation and competing solutes also impact adsorption. For example, with increasing Al content, Cismasu *et al.*⁴⁴ found that natural ferrihydrite samples with high Al and Si content tended to form aggregates and have lower surface area than pure ferrihydrite (as low as 65 m² g^{−1} in ferrihydrite with many impurities, down from 312 m² g^{−1} in ferrihydrite with fewer impurities). In the present study, higher amounts of Al only substantially decreased total U retention in the presence of Ca, suggesting that aggregation resulting from Al substitution did not appreciably decrease U adsorption site availability. There were also no competing solutes such as phosphate or silicate in this study, which have been shown to limit mineral transformation^{41,42} and U incorporation⁷ by blocking reactive surface sites or preventing recrystallization. Uranium adsorption site availability was therefore not a limiting factor for any of the Al loadings, lending support to the effect of Al on mineral transformation (*via* lattice changes, stress/strain, *etc.*) as the primary control on the U retention mechanism.

A secondary result of the increased prevalence of U adsorption over incorporation at high (10–20%) Al content was a decrease in overall U retention in the presence of 4 mM Ca²⁺. Our results are consistent with the observation of Stewart *et al.*¹⁶ that conditions in which the uranyl–calcium–carbonate ternary complex is dominant in solution result in an order of magnitude increase of solution-phase U. Ergo, decreasing U incorporation with increasing Al content is of particular concern in groundwater rich in Ca, due to lower U retention (*via* adsorption or incorporation).

In summary, the presence of Al³⁺ in ferrihydrite did not completely inhibit U incorporation into goethite resulting from Fe(II)-induced ferrihydrite transformation, even at Al contents as high as 20%. However, the extent of U incorporation decreased substantially with increasing Al content. Decreased U incorporation was due to the decrease of Al-ferrihydrite transformation to goethite and incompatibilities between the Al-

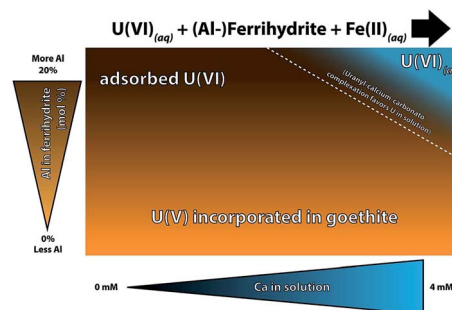


Fig. 5 Conceptual illustration of the effects of Al substitution in ferrihydrite/goethite and aqueous Ca concentration on U fate for the reaction of U(VI) with (Al-)ferrihydrite and Fe(II). The amount of U (as U(V)) incorporated into Al-goethite decreases with increasing Al content. Increased Ca concentration decreases U(VI) adsorption and when coupled with Al incorporation in ferrihydrite/goethite leads to greater aqueous U concentration (*i.e.*, less retention).

goethite lattice and incorporated U. The shift toward U adsorption and a corresponding decrease of U incorporation due to structural Al also resulted in increased U in solution in the presence of Ca^{2+} (Fig. 5).

Acknowledgements

Support for M.M. was provided partially by the Robert and Marvel Kirby Stanford Graduate Fellowship. Additionally, this research was supported by the U.S. Department of Energy Office of Biological and Environmental Research, through the Subsurface Biogeochemical Research program (grant number DE-SC0006772) and the SLAC Science Focus Area Research Program (FWP #10094). Use of the Stanford Synchrotron Radiation Lightsource, SLAC National Accelerator Laboratory, is supported by the U.S. Department of Energy, Office of Science, Office of Basic Energy Sciences under Contract no. DE-AC02-76SF00515. The contents of this publication are solely the responsibility of the authors and do not necessarily represent the official views of NIGMS, NCRR or NIH. Use of the Advanced Photon Source, an Office of Science User Facility operated for the U.S. Department of Energy (DOE) Office of Science by Argonne National Laboratory, was supported by the U.S. DOE under Contract no. DE-AC02-06CH11357. We wish to thank the technical staff on APS BL ID-11-B for their support. We thank Moses Gonzalez, Guangchao Li, and John Bargar for their assistance with this research, and two anonymous reviewers for their contributions that substantially improved the manuscript. We also appreciate the technical and safety support provided by L. Amoroso, D. Day, A. Gooch, D. Menke, C. Morris, D. Murray, C. Patty, and R. Russ.

References

- 1 IAEA, *The long term stabilization of uranium mill tailings*, International Atomic Energy Agency, 2004.
- 2 DOE, *Linking Legacies: Connecting the Cold War Nuclear Weapons Production Processes To Their Environmental Consequences*, US Department of Energy, 1997.
- 3 R. Riley and J. Zachara, *Chemical contaminants on DOE lands and selection of contaminant mixtures for subsurface science research*, 1992.
- 4 M. Duff, J. Coughlin and D. Hunter, *Geochim. Cosmochim. Acta*, 2002, **66**, 3533–3547.
- 5 E. S. Ilton, J. S. L. Pacheco, J. R. Bargar, Z. Shi, J. Liu, L. Kovarik, M. H. Engelhard and A. R. Felmy, *Environ. Sci. Technol.*, 2012, **46**, 9428–9436.
- 6 P. S. Nico, B. D. Stewart and S. Fendorf, *Environ. Sci. Technol.*, 2009, **43**, 7391–7396.
- 7 D. D. Boland, R. N. Collins, T. E. Payne and T. D. Waite, *Environ. Sci. Technol.*, 2011, **45**, 1327–1333.
- 8 M. S. Massey, J. S. Lezama-Pacheco, M. E. Jones, E. S. Ilton, J. M. Cerrato, J. R. Bargar and S. Fendorf, *Geochim. Cosmochim. Acta*, 2014, DOI: 10.1016/j.gca.2014.07.016.
- 9 T. D. Waite, J. A. Davis, T. E. Payne, G. A. Waychunas and N. Xu, *Geochim. Cosmochim. Acta*, 1994, **58**, 5465–5478.
- 10 J. Bargar, R. Reitmeyer and J. Davis, *Environ. Sci. Technol.*, 1999, **33**, 2481–2484.
- 11 D. Giammar and J. Hering, *Environ. Sci. Technol.*, 2001, **35**, 3332–3337.
- 12 T. Hiemstra, W. H. Van Riemsdijk, A. Rossberg and K.-U. Ulrich, *Geochim. Cosmochim. Acta*, 2009, **73**, 4437–4451.
- 13 D. M. Singer, K. Maher and G. E. Brown Jr, *Geochim. Cosmochim. Acta*, 2009, **73**, 5989–6007.
- 14 E. S. Ilton, Z. Wang, J.-F. Boily, O. Qafoku, K. M. Rosso and S. C. Smith, *Environ. Sci. Technol.*, 2012, **46**, 6604–6611.
- 15 P. M. Fox, J. A. Davis and J. M. Zachara, *Geochim. Cosmochim. Acta*, 2006, **70**, 1379–1387.
- 16 B. D. Stewart, M. A. Mayes and S. Fendorf, *Environ. Sci. Technol.*, 2010, **44**, 928–934.
- 17 E. Liger, L. Charlet and P. Van Cappellen, *Geochim. Cosmochim. Acta*, 1999, **63**, 2939–2955.
- 18 B. Hua, H. Xu, J. Terry and B. Deng, *Environ. Sci. Technol.*, 2006, **40**, 4666–4671.
- 19 B. Hua and B. Deng, *Environ. Sci. Technol.*, 2008, **42**, 8703–8708.
- 20 D. E. Latta, C. A. Gorski, M. I. Boyanov, E. J. O'Loughlin, K. M. Kemner and M. M. Scherer, *Environ. Sci. Technol.*, 2012, **46**, 778–786.
- 21 X. Du, B. Boonchayaanant, W.-M. Wu, S. Fendorf, J. Bargar and C. S. Criddle, *Environ. Sci. Technol.*, 2011, **45**, 4718–4725.
- 22 D. R. Lovley and E. J. P. Phillips, *Environ. Sci. Technol.*, 1992, **26**, 2228–2234.
- 23 R. Anderson, H. Vrionis, I. Ortiz-Bernad, C. Resch, P. Long, R. Dayvault, K. Karp, S. Marutzky, D. Metzler, A. Peacock, D. White, M. Lowe and D. Lovley, *Appl. Environ. Microbiol.*, 2003, **69**, 5884–5891.
- 24 J. R. Lloyd, *FEMS Microbiol. Rev.*, 2003, **27**, 411–425.
- 25 W.-M. Wu, J. Carley, T. Gentry, M. Ginder-Vogel, M. Fienen, T. Mehlhorn, H. Yan, S. Carroll, M. Pace, J. Nyman, J. Luo, M. Gentile, M. Fields, R. Hickey, B. Gu, D. Watson, O. Cirpka, J. Zhou, S. Fendorf, P. Kitanidis, P. Jardine and C. Criddle, *Environ. Sci. Technol.*, 2006, **40**, 3986–3995.
- 26 J. D. Wall and L. R. Krumholz, *Annu. Rev. Microbiol.*, 2006, **60**, 149–166.
- 27 S. B. Yabusaki, Y. Fang, P. E. Long, C. T. Resch, A. D. Peacock, J. Komlos, P. R. Jaffe, S. J. Morrison, R. D. Dayvault, D. C. White and R. T. Anderson, *J. Contam. Hydrol.*, 2007, **93**, 216–235.
- 28 W.-M. Wu, J. Carley, J. Luo, M. Ginder-Vogel, E. Cardenas, M. Leigh, C. Hwang, S. Kelly, C. Ruan, L. Wu, J. Van Nostrand, T. Gentry, K. Lowe, S. Carroll, W. Luo, M. Fields, B. Gu, D. Watson, K. Kemner, T. Marsh, J. Tiedje, J. Zhou, S. Fendorf, P. Kitanidis, P. Jardine and C. Criddle, *Environ. Sci. Technol.*, 2007, **41**, 5716–5723.
- 29 H. R. Beller, *Appl. Environ. Microbiol.*, 2005, **71**, 2170–2174.
- 30 H. S. Moon, J. Komlos and P. R. Jaffe, *Environ. Sci. Technol.*, 2007, **41**, 4587–4592.
- 31 W.-M. Wu, J. Carley, S. J. Green, J. Luo, S. D. Kelly, J. V. Nostrand, K. Lowe, T. Mehlhorn, S. Carroll, B. Boonchayaanant, F. E. Löffler, D. Watson, K. M. Kemner, J. Zhou, P. K. Kitanidis, J. E. Kostka, P. M. Jardine and C. S. Criddle, *Environ. Sci. Technol.*, 2010, **44**, 5104–5111.

- 32 M. Ginder-Vogel, B. Stewart and S. Fendorf, *Environ. Sci. Technol.*, 2010, **44**, 163–169.
- 33 Z. Wang, S.-W. Lee, P. Kapoor, B. M. Tebo and D. E. Giammar, *Geochim. Cosmochim. Acta*, 2013, **100**, 24–40.
- 34 B. D. Stewart, P. S. Nico and S. Fendorf, *Environ. Sci. Technol.*, 2009, **43**, 4922–4927.
- 35 S. Kerisit, A. R. Felmy and E. S. Ilton, *Environ. Sci. Technol.*, 2011, **45**, 2770–2776.
- 36 P. Gómez, A. Garralón, B. Buil, M. J. Turrero, L. Sánchez and B. de la Cruz, *Sci. Total Environ.*, 2006, **366**, 295–309.
- 37 J. C. Pett-Ridge, V. M. Monastera, L. A. Derry and O. A. Chadwick, *Chem. Geol.*, 2007, **244**, 691–707.
- 38 C. Hansel, S. Benner, J. Neiss, A. Dohnalkova, R. Kukkadapu and S. Fendorf, *Geochim. Cosmochim. Acta*, 2003, **67**, 2977–2992.
- 39 C. M. Hansel, S. G. Benner and S. Fendorf, *Environ. Sci. Technol.*, 2005, **39**, 7147–7153.
- 40 H. D. Pedersen, D. Postma, R. Jakobsen and O. Larsen, *Geochim. Cosmochim. Acta*, 2005, **69**, 3967–3977.
- 41 T. Borch, Y. Masue, R. K. Kukkadapu and S. Fendorf, *Environ. Sci. Technol.*, 2007, **41**, 166–172.
- 42 A. M. Jones, R. N. Collins, J. Rose and T. D. Waite, *Geochim. Cosmochim. Acta*, 2009, **73**, 4409–4422.
- 43 R. M. Cornell and U. Schwertmann, *The Iron Oxides: Structure, Properties, Reactions, Occurrences, and Uses*, Wiley-VCH GmbH & Co. KGaA, 2nd edn, 2003.
- 44 A. C. Cismasu, F. M. Michel, A. P. Tcaciuc, T. Tyliszczak and G. E. Brown Jr, *C. R. Geosci.*, 2011, **343**, 210–218.
- 45 A. C. Cismasu, F. M. Michel, J. F. Stebbins, C. Levard and G. E. Brown Jr, *Geochim. Cosmochim. Acta*, 2012, **92**, 275–291.
- 46 Y. Masue-Slowey, R. H. Loeppert and S. Fendorf, *Geochim. Cosmochim. Acta*, 2011, **75**, 870–886.
- 47 C. M. Hansel, D. R. Learman, C. J. Lentini and E. B. Ekstrom, *Geochim. Cosmochim. Acta*, 2011, **75**, 4653–4666.
- 48 Y. Masue, R. H. Loeppert and T. A. Kramer, *Environ. Sci. Technol.*, 2007, **41**, 837–842.
- 49 S. M. Webb, *Phys. Scr.*, 2005, 1011.
- 50 B. Ravel and M. Newville, *J. Synchrotron Radiat.*, 2005, **12**, 537–541.
- 51 S. Zabinsky, J. Rehr, A. Ankudinov, R. Albers and M. Eller, *Phys. Rev. B: Condens. Matter Mater. Phys.*, 1995, **52**, 2995–3009.
- 52 A. L. Ankudinov, J. J. Rehr and S. D. Conradson, *Phys. Rev. B: Condens. Matter Mater. Phys.*, 1998, **58**, 7565–7576.
- 53 A. C. Larson and R. B. Von Dreele, *GSAS*, Los Alamos National Laboratory, 2000.
- 54 B. Toby, *J. Appl. Crystallogr.*, 2001, **34**, 210–213.
- 55 K. M. Campbell, H. Veeramani, K.-U. Ulrich, L. Y. Blue, D. E. Giammar, R. Bernier-Latmani, J. E. Stubbs, E. Suvorova, S. Yabusaki, J. S. Lezama-Pacheco, A. Mehta, P. E. Long and J. R. Bargar, *Environ. Sci. Technol.*, 2011, **45**, 8748–8754.
- 56 E. Bazilevskaya, D. D. Archibald, M. Aryanpour, J. D. Kubicki and C. E. Martinez, *Geochim. Cosmochim. Acta*, 2011, **75**, 4667–4683.
- 57 S. V. Yanina and K. M. Rosso, *Science*, 2008, **320**, 218–222.
- 58 R. M. Handler, B. L. Beard, C. M. Johnson and M. M. Scherer, *Environ. Sci. Technol.*, 2009, **43**, 1102–1107.
- 59 K. M. Rosso, S. V. Yanina, C. A. Gorski, P. Larese-Casanova and M. M. Scherer, *Environ. Sci. Technol.*, 2010, **44**, 61–67.
- 60 D. E. Latta, J. E. Bachman and M. M. Scherer, *Environ. Sci. Technol.*, 2012, **46**, 10614–10623.
- 61 S. A. Crosby, D. R. Glasson, A. H. Cuttler, I. Butler, D. R. Turner, M. Whitfield and G. E. Millward, *Environ. Sci. Technol.*, 1983, **17**, 709–713.
- 62 J.-H. Jang, B. A. Dempsey and W. D. Burgos, *Environ. Sci. Technol.*, 2007, **41**, 4305–4310.
- 63 E. E. Roden and J. M. Zachara, *Environ. Sci. Technol.*, 1996, **30**, 1618–1628.